Presented at: SAMPE 2010 Conference
Seattle, WA, May 17-20, 2010

COMPOSITE NDE USING QUASISTATIC ELECTROMAGNETIC METHODS

Andrew Washabaugh, David Grundy, Neil Goldfine
JENTEK Sensors, Inc., 110-1 Clematis Avenue, Waltham, MA 02453-7013

ABSTRACT

Composite components are now used in a wide variety of structural applications due to their excellent specific strength and stiffness, and improvements in costs and manufacturing quality. Representative applications include aircraft/rotorcraft, spacecraft, ships, and wind turbines. Often, the composites are used to replace metal components, but life management for composites is in its infancy compared to life management for metal structures. In part, this is due to limitations in the ability of standard nondestructive evaluation (NDE) methods to adequately observe manufacturing quality conditions and to observe in-service damage progression.

This paper describes recent developments in quasistatic (relatively low frequency, 100 kHz – 40 MHz) electromagnetic methods for the examination and assessment of composite condition. This includes application of Meandering Winding Magnetometer (MWM®) (magnetic field) sensing methods for carbon fiber composites and Interdigitated Electrode Dielectrometer (IDED™) (electric field) sensing methods for glass fiber reinforced composites and ceramic matrix composites. These methods use physics-based models to relate sensor responses to properties of the matrix, fibers, and bonding conditions, and, in some applications, high-spatial resolution imaging. This facilitates NDE for both scanning and surface mounted sensors for damage, condition, stress and temperature monitoring for both in-service assessment and during manufacturing quality control.

1. INTRODUCTION

The increasing use of composite components in structural applications requires nondestructive evaluation (NDE) methods that can ensure structural integrity over the life-time of these components. However, limitations in the ability of standard NDE methods to observe manufacturing quality variations and in-service damage evolution of composite structures can prevent designers from realizing the full potential of composite materials. Recent developments of model-based quasistatic (low frequency) electromagnetic methods for the examination and assessment of composite condition address some of these limitations.

1.1 Scope

This paper describes technologies and methods related to NDE and structural health monitoring for both damage inspection and assessment of material condition. The focus of the paper is magnetic field or eddy current sensing methods for composites having conducting fibers, such as graphite fiber composites, but the application of these techniques to electric field assessment of weakly conducting or insulating composites, such as fiberglass, is also discussed. This paper describes some measurements that were performed on composite panels to demonstrate sensitivity to impact damage and stress variation with mechanical loading. A micromechanical model for the composite response is also described.

1.2 Background

While NDE has been shown to play an important role in ensuring the integrity of large bonded structures [1], most methods provide only an indication of the presence of damage; information about the defect characteristics are limited and often insufficient for detection of damage early enough to avoid failures or to enable cost effective condition based maintenance. Furthermore, the complex internal structures of

Copyright 2010 by JENTEK Sensors, Inc. Published by Society for the Advancement of Material and Process Engineering with permission.

composites introduce new requirements for observability of internal and interfacial stresses that cannot be delivered by conventional strain gages or other means.

Damage to composite components can result from a variety of causes. A very common cause is foreign object damage, from an impact, such as hail strikes or other debris strikes. This impact damage can cause matrix cracking or filament rupture, delamination, or disbonds. Damage can also result from overload situations where excessive mechanical loads are applied to the composite. Built-up structures, including metal-composite joints introduce additional complexity. While composites have revolutionized structural design and manufacturing, fastening/joining and design methodologies that are artifacts of metallic aircraft life management experience continue to be used. Risk mitigation dictates life management behavior because of limitations in the ability to observe manufacturing quality and in-service damage evolution. This is the case for widely used graphite fiber composite constructs, metal/composite laminates and joints, and more advanced composites such as ceramic and metal matrix composites.

2. EXPERIMENTATION

2.1 Samples and Apparatus

Measurements were performed on graphite fiber/epoxy composite panels. These panels were provided by Lockheed Martin in support of a NAVAIR funded SBIR program. Figure 1 shows a photograph of an undamaged composite panel installed in a scanning fixture. An MWM-Array is mounted under the probe electronics (shown in the photograph) and placed against the panel during testing. The response of each sense element was measured using JENTEK's 39-channel impedance instrumentation and GridStation® data acquisition and analysis software. The scanner incorporates a linear position encoder to provide the array position during the scan. The sensor was calibrated using measurements of the sensor response in air. The data on the composite panel was converted into an effective conductivity and lift-off using grid-based inverse methods, as described below, assuming an infinite half-space of a homogeneous test material.

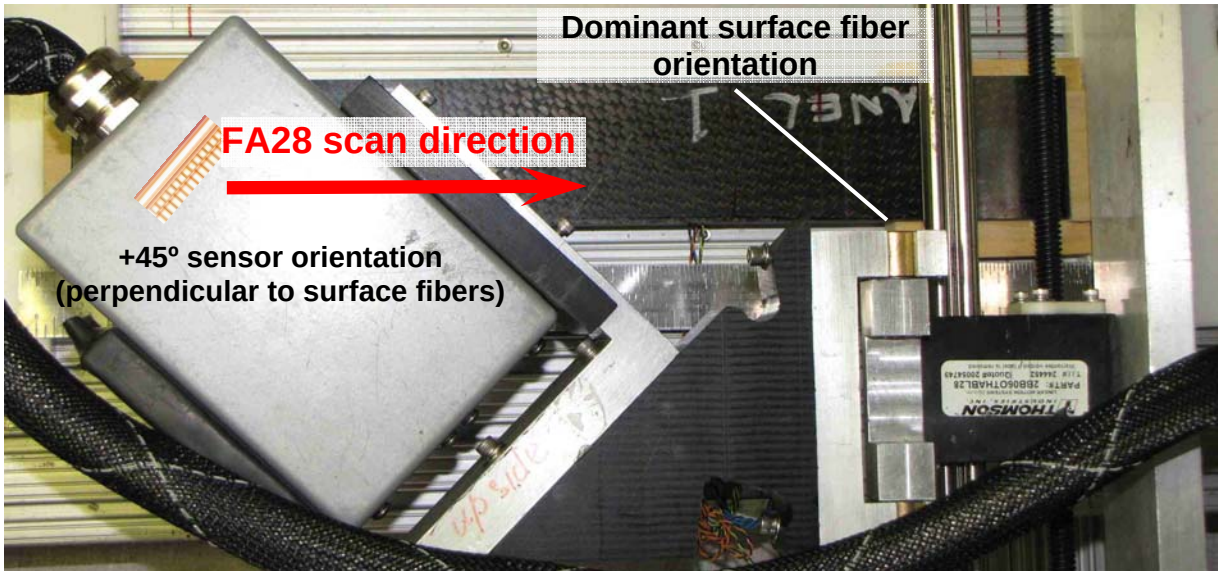

Figure 1. Photograph (top view, looking down) of a graphite fiber/epoxy composite panel in a scanning apparatus. The FA28 MWM-Array is located between the probe electronics (pictured on the left) and the composite panel. In this orientation the MWM-Array is perpendicular to the surface fibers and at a 45º sensor orientation with respect to the panel edge.

2.2 Magnetoquasistatic Sensing: The Meandering Winding Magnetometer (MWM®)

The MWM-Arrays are thin and conformable eddy current sensor arrays that can be scanned across a surface, mounted on an exposed surface, or embedded between layers of a joint or into a composite [2-4]. Three example MWM-Array configurations are shown in Figure 2. The windings of the MWM-Arrays are designed so that the magnetic field interaction with the test material can be modeled accurately. This can significantly reduce calibration requirements. In some situations an "air calibration" can be used, where a measurement of the sensor response in air can be used to calibrate the sensor response, permitting measurement of a component's absolute electrical conductivity without calibration standards. The distance between the sense element and the primary is proportional to the spatial wavelength of the sensor array and can be selected to adjust the sensitivity to near-surface property variations.

For the MWM-Arrays, the surface fiber orientation can affect the measurements depending upon the sensor geometry that is chosen. For example, for a small spatial wavelength sensor the corresponding depth of penetration of the interrogating magnetic field is small and the sensor will dominantly respond to the surface fibers. In contrast for a large spatial wavelength sensor, the sensor will respond to properties throughout the bulk of the panel and should be less sensitive to surface fiber orientation effects. For comparison, the FA28, shown in Figure 2 (left), has two rectangular drive windings placed adjacent to each other and a linear array of thirty-seven, 1 mm (0.040-in.) square, sense elements. This provides a scan width for the sense element array of 37 mm (1.48-in.). The linear array of sense elements is centered inside one of the drive windings so that the gap between the sense elements and the drive winding is only 0.25 mm (0.010 in.). In contrast, the FA24, shown in Figure 2 (right), has two rectangular drive windings placed adjacent to each other and a linear array of thirty-seven, 2.5 mm (0.10-in.) wide sense elements. This provides a net width of the sense element array of 92.5 mm (3.7-in.). The gap between the sense elements and the drive winding is 2 mm (0.080-in.).

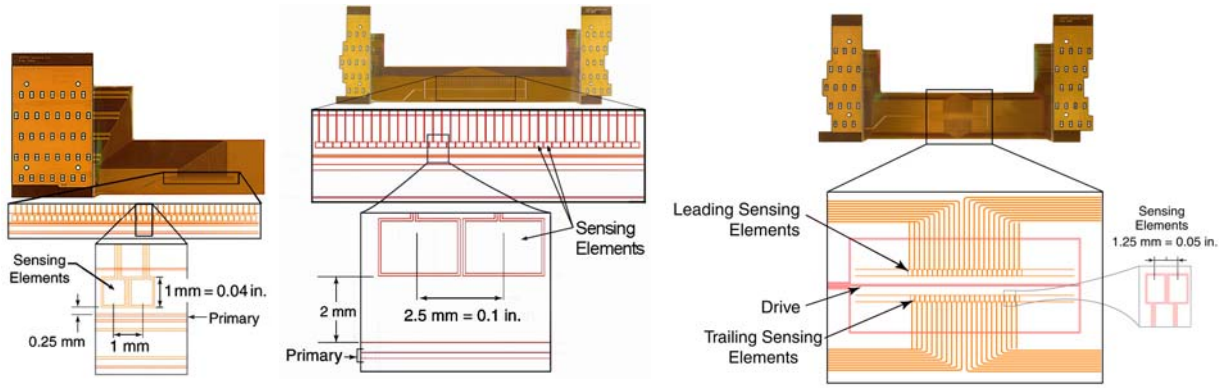

FA28 FA24 FA26

Figure 2. Photographs of MWM-Arrays. (Left) FA28, (middle) FA24, (right) FA26.

Figure 3 shows a plot of the depth of penetration of the magnetic fields for an FA24 (large spatial wavelength sensor) and an FA28 (small spatial wavelength sensor). The depth of penetration is obtained from

$$SDP = 1/\mathrm{Re}\left[\sqrt{\left(\frac{2\pi}{\lambda}\right)^2 + j\frac{2}{\delta^2}}\right] \quad ; \quad \delta = \sqrt{\frac{2}{\omega\mu\sigma}} \qquad (1)$$

with λ the spatial wavelength for the sensor and δ the skin depth, ω the angular frequency, μ the magnetic permeability and σ the electrical conductivity. The depth of penetration is dominated by the shorter of the spatial wavelength or the skin depth. For the FA24 the larger depth of penetration is based on the dimensions of the drive winding and reflects the fundamental spatial mode for the applied magnetic field while the smaller depth of penetration is based on the distance between the drive winding and the sense

elements and reflects the depth of penetration of the components of the magnetic field dominantly coupled to the sense element. With a typical graphite fiber/epoxy composite electrical conductivity of order 0.01%IACS (5.8 kS/m), the depth of penetration is determined primarily by the sensor spatial wavelength. The FA24 can respond to bulk property variations and damage but the FA28 will respond primarily to near-surface properties within several plies of the surface nearest the sensor. Figure 1 also shows the sensor orientation with respect to the panel edge. The fibers at the surface are dominantly at a -45º orientation. Thus, a sensor orientation of +45º has the drive winding perpendicular to the fibers at the surface. In the lower half of the first ply, the fibers are parallel to the drive. The second ply layer is oriented at 0º and the fibers are oriented at 45º to the sensor. The third ply has a half-ply of fibers parallel to the drive over a half-ply of fibers perpendicular to the drive winding. The fourth ply is similar to the second ply. This layup then repeats for the remaining plies. Thus, since the FA28 has a relatively small spatial wavelength (i.e., the depth of penetration is limited) an orientation dependence is expected in the response.

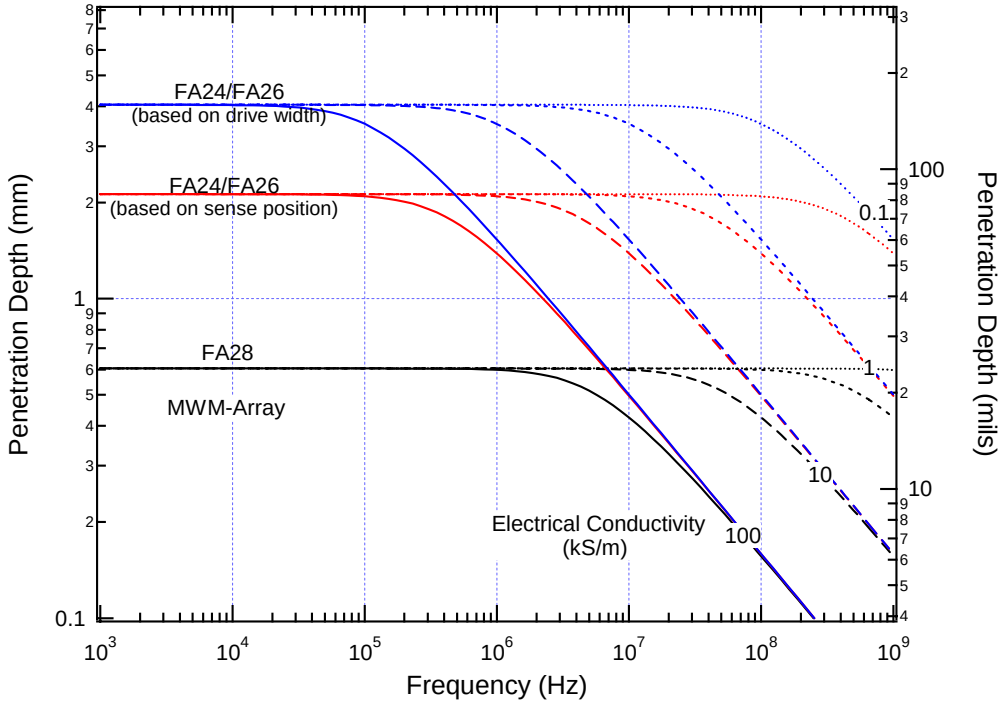

Figure 3. Depth of penetration plot for several MWM-Arrays. The FA28 has a small spatial wavelength while the FA24/FA26 has a large spatial wavelength.

2.3 Grid-based Inversion Methods

The MWM and IDED sensor responses are converted into material or geometric properties using measurement grids [4]. These grids are used to convert two known values, such as the magnitude and phase (or real and imaginary parts) of the transimpedance, into the unknown properties of interest, such as electrical conductivity and lift-off. The grids are generated using a forward model and properties of the test material to create two-dimensional databases, or precomputed responses, which can be displayed graphically to support procedure development. Figure 4 shows conductivity/lift-off grids at three different frequencies. Higher order databases are used for the determination of more than two unknown properties of interest.

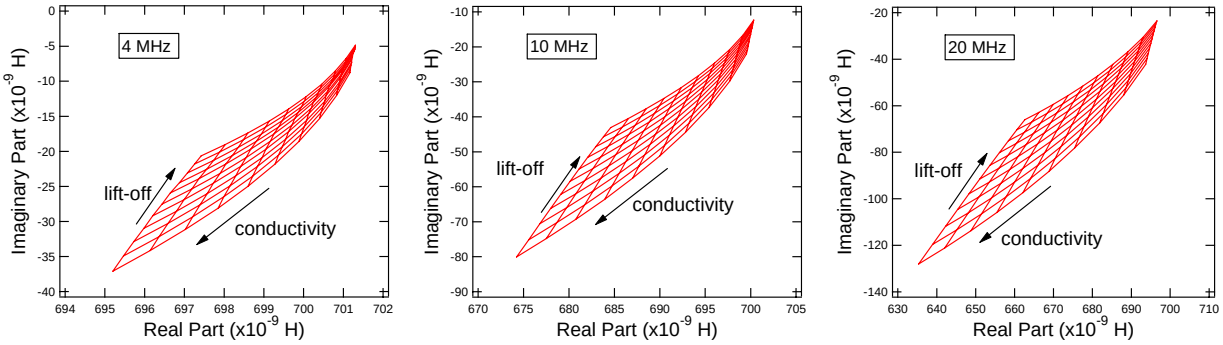

Figure 4: FA28 conductivity/lift-off grids, (4 MHz - left, 10 MHz – middle, 20 MHz - right).

3. RESULTS

This section describes the results from two types of measurements. The first section describes eddy current imaging of impact damage while the second section describes assessment of bending stress in a mechanically loaded panel.

3.1 Imaging of Impact Damage in a Composite Panel

3.1.1 FA28 (Short Spatial Wavelength) Scans

A short spatial wavelength FA28 MWM-Array was used to examine a damaged graphite fiber/epoxy composite panel. For these scans, three pieces of tape were placed against the surface to help register the images with respect to the damage. The data on the composite panel was converted into an effective conductivity and lift-off using measurement grids that assumed an infinite half-space of a homogeneous test material.

Figure 5 shows effective property images for an FA28 oriented perpendicular to the surface fibers. For this orientation, a 0.004-in. thick layer of Teflon tape was added to the sensor in order to move the sensor responses so that the measurement data fell within the measurement grid and yielded reasonable physical values. The average conductivity and lift-off values are consistent across the frequency range. There are distinct variations in the images that may be consistent with the presence of property variations in hidden fiber tows. At the impact damage site, near the center of the panel, there appears to be a region of reduced conductivity. Note that in these images the scotch tape stands out in the lift-off images, but not in the conductivity images, which demonstrates independence in the conductivity and lift-off measurement.

Figure 6 shows the corresponding effective properties for an FA28 oriented parallel to the surface fibers for the composite panel. In these images, the spatial variations in the conductivity and lift-off are consistent with the width of the fiber tows. The same color scale was used for the effective conductivity images so that there is a visible reduction in the effective conductivity with frequency over the entire panel. There is also a visible reduction in the average lift-off for each panel as the frequency increases.

Figure 7 shows the effective properties for an FA28 oriented at an angle of +45º with respect to the surface fibers. Similar results were obtained for a FA28 orientation of -45º. The effective conductivity decreases modestly with increasing frequency, but the effective lift-off is relatively large and decreases significantly with lift-off. The presence of the fiber tows are relatively difficult to see in these images. However, the damage appears to be visible in the higher frequency conductivity data and in the lift-off images.

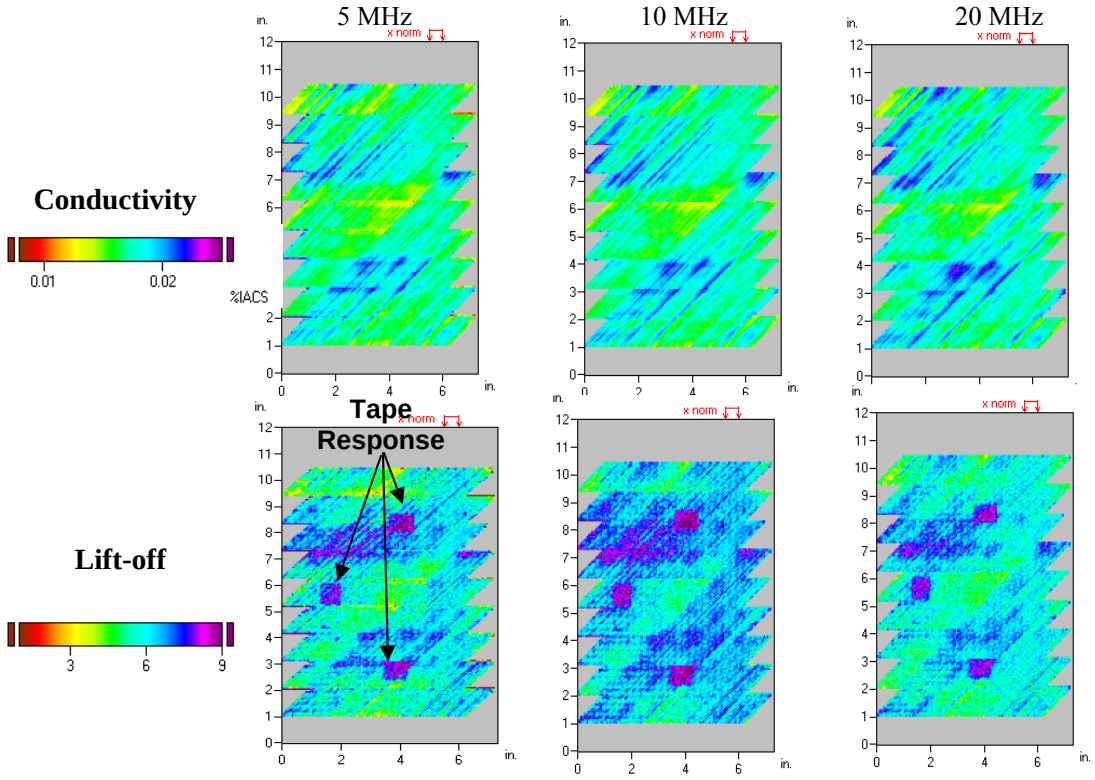

Figure 5. Effective property images for an impact damage panel with an FA28 oriented perpendicular to the surface fibers (+45º sensor orientation with respect to panel edge).

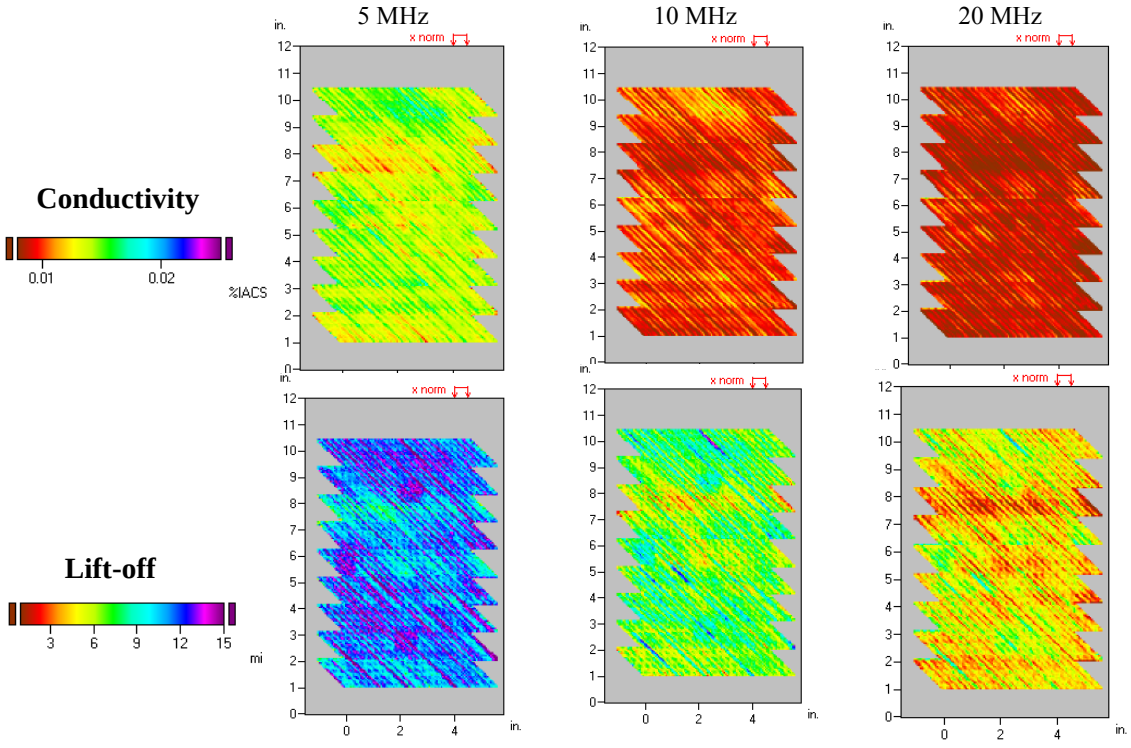

Figure 6. Effective property images for an impact damage panel with an FA28 oriented parallel to the surface fibers (-45º sensor orientation with respect to panel edge).

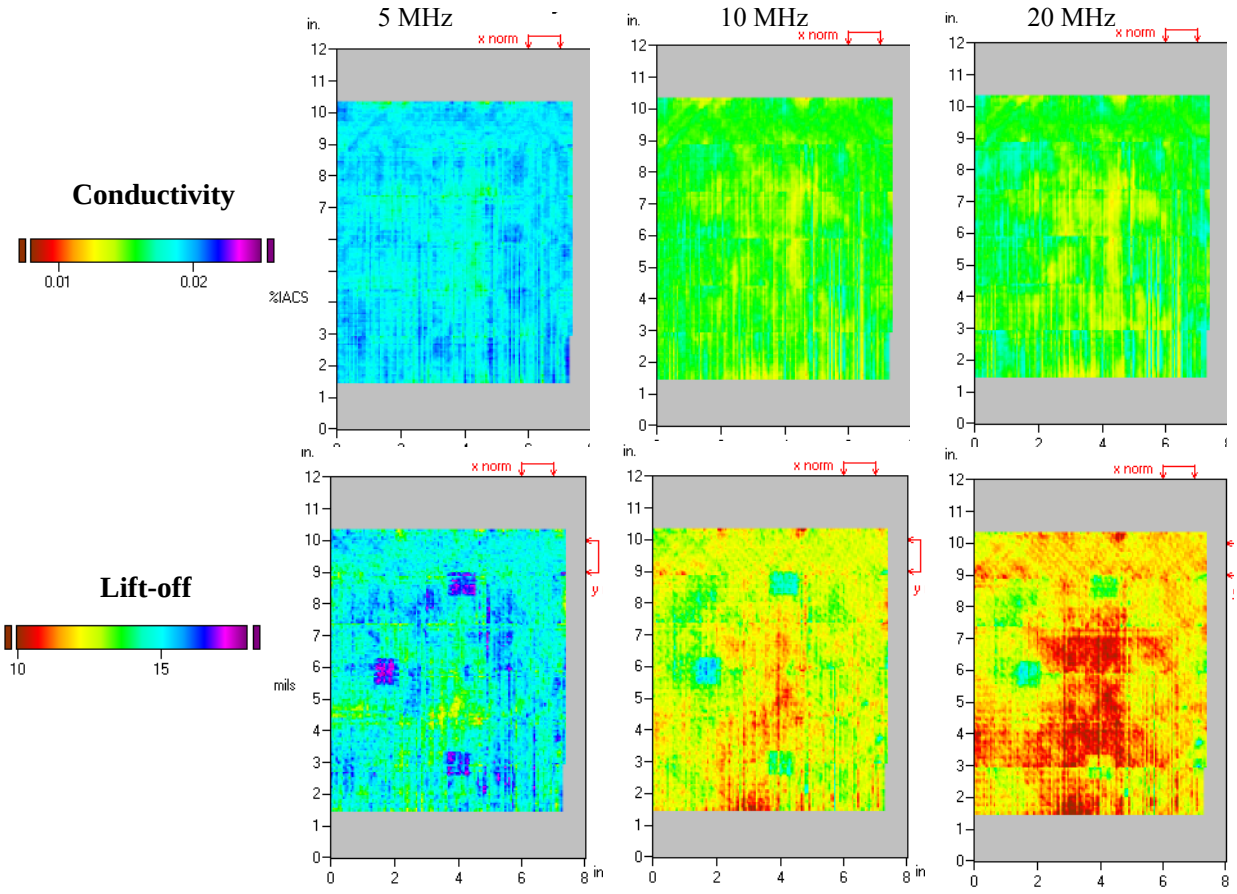

Figure 7. Effective property images for an impact damage panel with an FA28 oriented at a 45º angle to the surface fibers (0º sensor orientation with respect to panel edge).

3.1.2 FA26 (Long Spatial Wavelength) Scans

The same damaged graphite fiber/epoxy composite panel was also examined with a longer spatial wavelength FA26 MWM-Array. This MWM-Array has the same basic geometry of the FA24 shown in Figure 2(right) except for the sense element width; the FA26 has 1.3 mm (0.050-in.) wide sense elements while the FA24 has 2.5 mm (0.10-in.) wide sense elements. This allows the FA26 to create slightly higher spatial resolution images than the FA24.

Figure 8 shows the effective property images for an FA26 oriented perpendicular to the surface fibers. As with the FA28 data of Figure 5, the average conductivity and lift-off values are consistent across the frequency range. There is also a distinct reduction in the effective property values at all frequencies in the vicinity of the impact damage. Around the lower piece of tape, outside the nominal damage region, there is a modest increase in the conductivity and lift-off. This may be due to the impact damage itself or possibly residual stress variations in the composite.

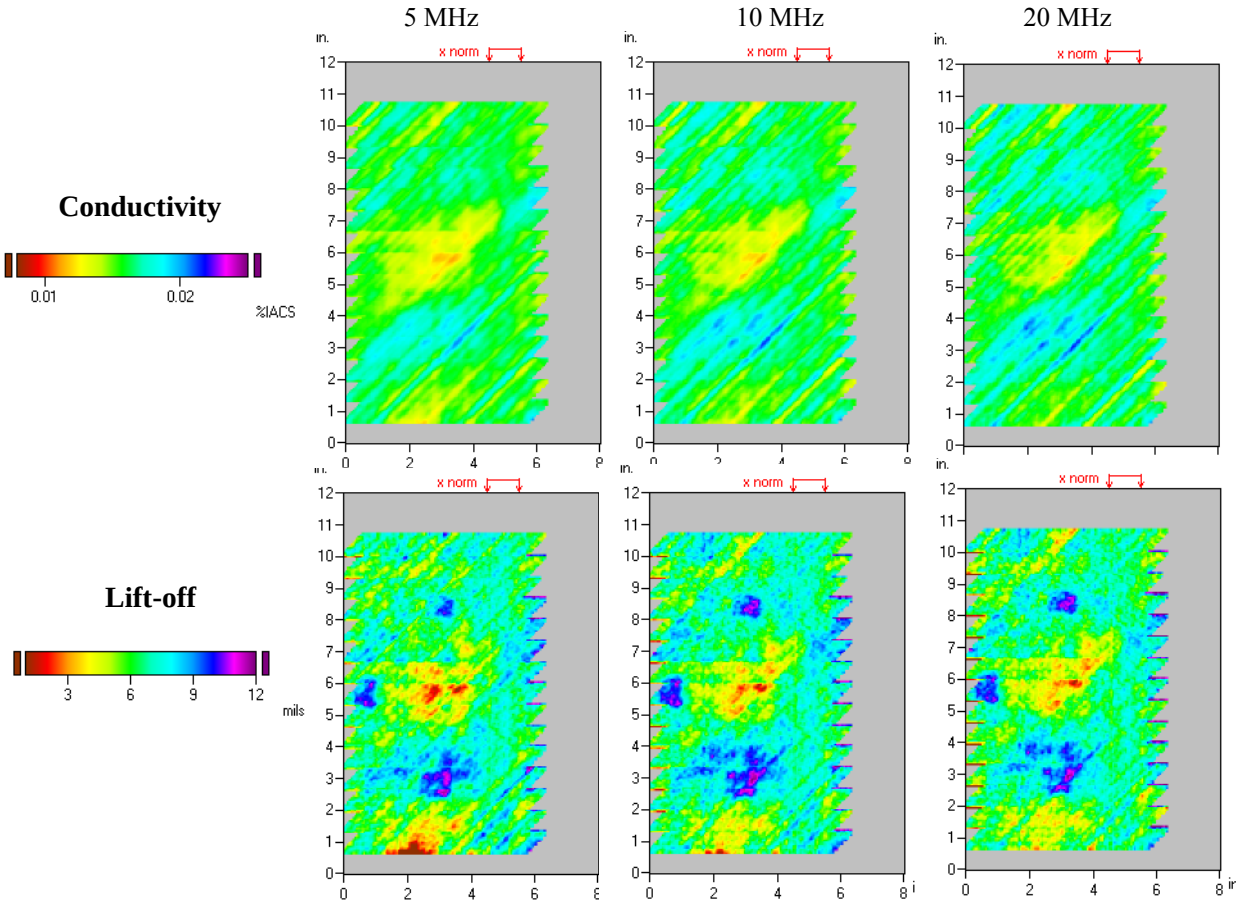

Figure 8. Effective property images for an impact damage panel with an FA26 oriented perpendicular to the surface fibers (+45º sensor orientation with respect to panel edge).

Figure 9 shows effective property images for an FA26 oriented parallel to the surface fibers for the composite panel. Similar to the shorter spatial wavelength measurements, there is a periodic variation in the effective properties consistent with the presence of the fiber tows. While the pieces of tape are not apparent in the lift-off images, the impact damage area appear as a local reduction in the conductivity and lift-off values. This reduction in effective property values was **not** observed with the FA28 images of Figure 6, which suggests that the damage is subsurface. It is our understanding that such subsurface fiber damage is typical of such impacts in composites. (Recall that the FA28 has a shorter spatial wavelength than the FA26 and is not sensitive to the deeper material property variations that can be sensed with the FA26.) This indicates that multiple spatial wavelength MWM-Arrays can be used to determine the depth of damage in graphite fiber/epoxy composites.

Figure 10 shows the effective properties for an FA26 oriented at an angle of +45º with respect to the surface fibers. Similar results were obtained for a FA26 orientation of -45º. In both of these orientations, the effective conductivity and lift-off decrease modestly with increasing frequency. The tape pieces are difficult to see in the images, but the impact damage area near the center of the images is visible. The damage tends to appear as a local reduction in the conductivity.

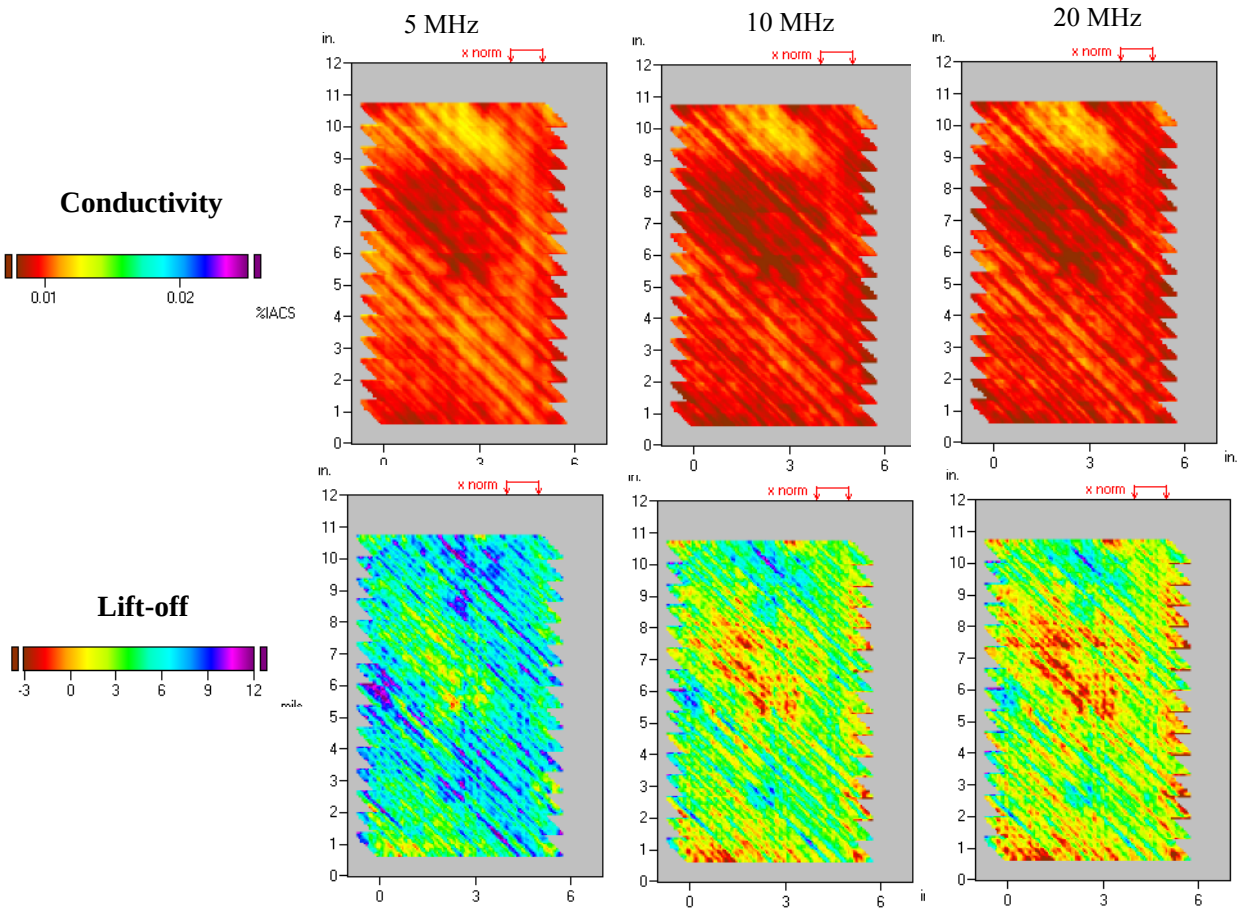

Figure 9. Effective property images for an impact damage panel with an FA28 oriented parallel to the surface fibers (-45º sensor orientation with respect to panel edge).

3.2 Mechanically Loaded Undamaged Composite Panel

Measurements were performed on a composite strip specimen to monitor property changes with loading. In this case, a 2.25-in. wide composite strip was mounted in a 4-point bend fixture which had steel screws at the ends for applying a controlled load. Strain gages were mounted on the back of the panel to provide a means for assessing the applied load. The probe electronics was mounted in an x-y scanner to facilitate repeatable scan images over the central area of the strip. This set of measurements was performed with an FA28 since it has a small spatial wavelength and should be more sensitive to stress variations in the upper plies; the next section shows measurement results obtained for an FA26.

Figure 11 shows effective conductivity images for three sensor orientations taken along the center of the strip. The bending stress was varied between scans as indicated in the figure. The spatial variation in the effective conductivity is consistently observed and appears to be associated with the periodicity of the fabric tows. This spatial variation in the conductivity appears to mask the conductivity variation associated with the stress, but in these orientations the average conductivity appears to increase slightly with increasing stress.

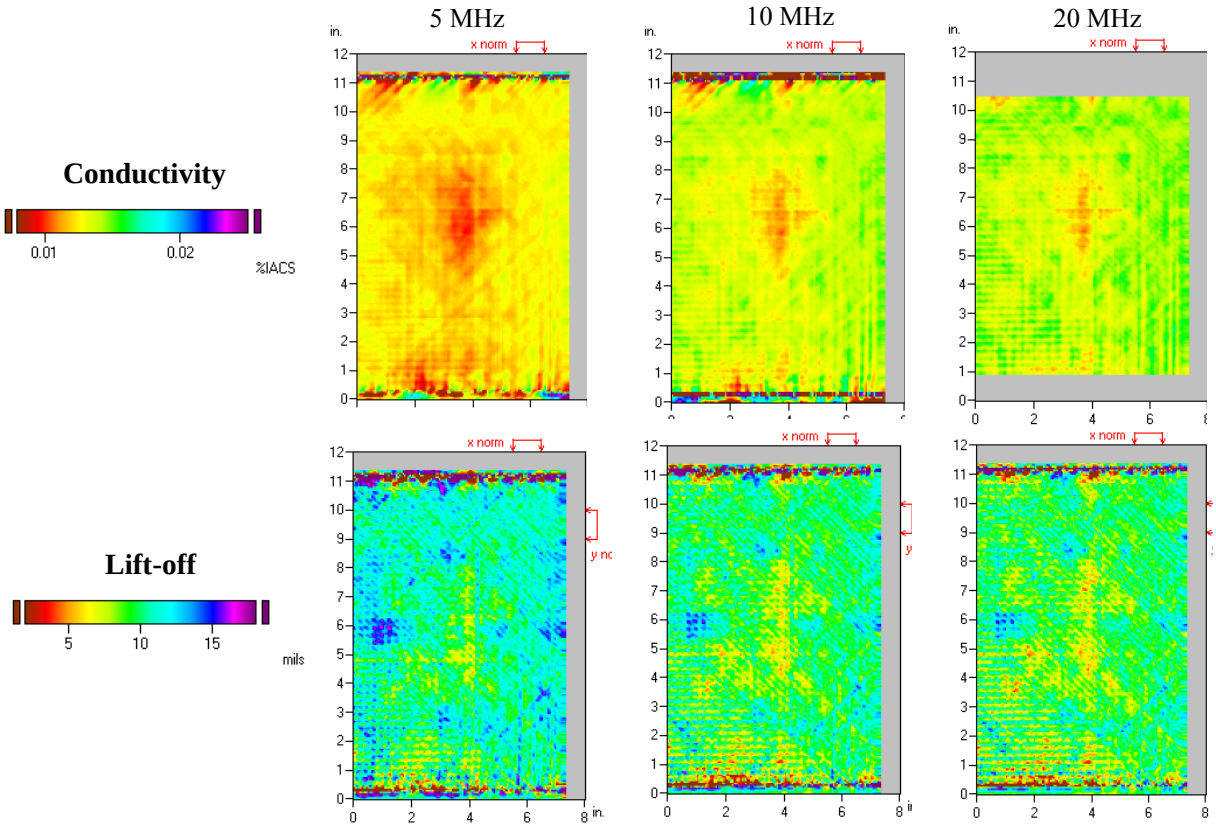

Figure 10. Effective property images for an impact damage panel with an FA26 oriented at a 45º angle to the surface fibers (0º sensor orientation with respect to panel edge).

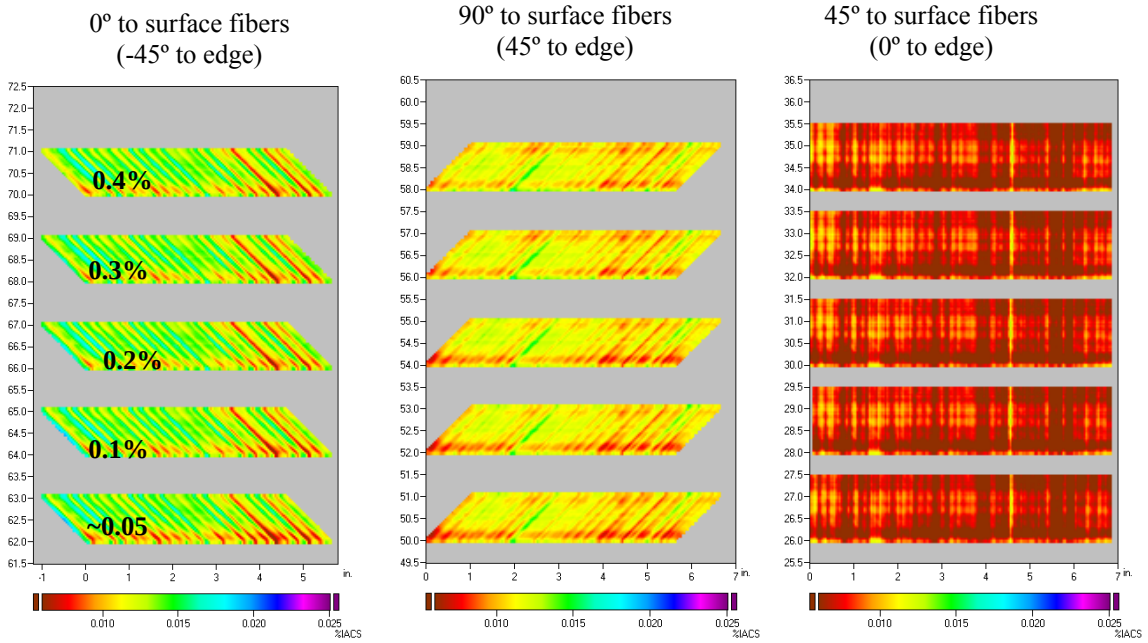

Figure 11. Effective conductivity images as the bending strain is varied for an FA28 at 12.5 MHz and for three sensor orientations.

Figure 12 shows a plot of the change in conductivity, relative to the initial state, for each sensor orientation at 12.6 MHz. Although spatial variations are observed in each scan image, only the average conductivity was used for this calculation. The conductivity change is within the range of what is expected from the literature, such as up to 5% conductivity change with a strain of 0.3%. The polarity of the change, e.g., an increase or decrease in conductivity with strain, varies with the orientation and may reflect spatial variations in the strain and residual stress variations [5]. Since the bending stress (and strain) is largest at the surface and varies across the thickness of the composite and the response of the FA28 also varies with depth into the composite.

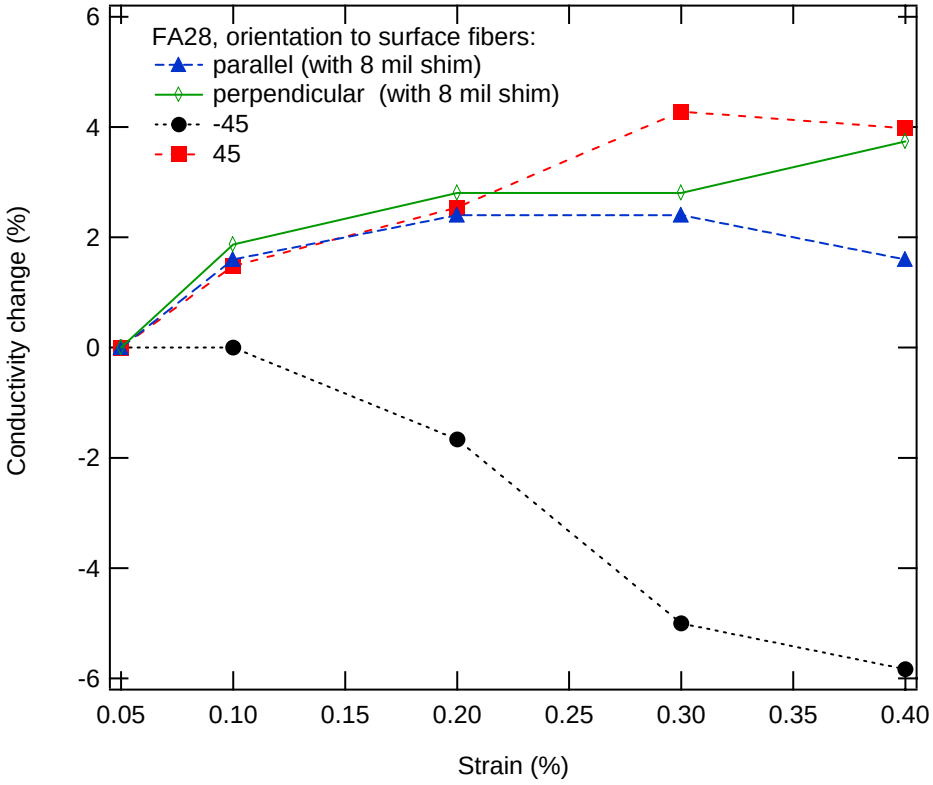

Figure 12. Composite conductivity change with bending strain for an FA28 at 12.6 MHz.

4. MICROMECHANICAL MODEL ANALYSIS

Micromechanical models are commonly used in mechanical and thermal analysis to predict stress, strain, and temperature variations throughout composite components and structures. For some NDE methods, such as ultrasonics, thermography, eddy-current, and dielectrometry, these models are also suitable for quantitatively determining properties of the constituents of the composite. For graphite fiber epoxy composites and eddy-current methods, the sensor response depends upon the sensor orientation with respect to the conducting fibers, the electrical conductivity and volume fraction of the fibers, and the thicknesses of the fabric layers. Expressions for the composite effective property variation with orientation can be obtained from a standard composite cylinder assemblage micromechanical model [6].

In each layer of the composite, it is assumed that the local magnetic field distribution is governed by the field orientation with respect to the fibers within the composite. Figure 13 shows a unidirectional fiber geometry for a collection of fibers. For a magnetic field-based sensor, the effective magnetic permeability and electrical conductivity of the matrix and fibers are the material properties of interest and depend upon the direction of the field with respect to the fibers. Here, it is assumed that the matrix is electrically insulating and non-magnetic. However, the fibers can be magnetic (relative permeability of μ) and conducting

(conductivity of σ_f). After solving for the field distribution around each fiber and applying the appropriate boundary condition, the anisotropic relative magnetic permeability in each orientation can be expressed as

$$\mu_{par} = \mu v_f + \mu_o v_m \tag{2}$$

$$\mu_{perp} = \mu_o \left\{ 1 + \frac{(\mu - \mu_o)(1 - v_m)}{\mu_o + (\mu - \mu_o)\frac{v_m}{2}} \right\} = \mu_o \left\{ \frac{\mu_o v_m + \mu(1 + v_f)}{\mu_o (1 + v_f) + \mu v_m} \right\} \tag{3}$$

with μ_o the permeability of free space, v the volume fraction of each material and where the subscript *m* denotes the matrix and *f* denotes the fibers. Note that $v_m = 1 - v_f$. In addition to the anisotropic effective magnetic permeability, the composite also has a direction-dependent ohmic conductivity:

$$\sigma_{par} = \sigma_f v_f + \sigma_m v_m \tag{4}$$

$$\sigma_{perp} = \sigma_m \left\{ 1 + \frac{(\sigma_f - \sigma_m)(1 - v_m)}{\sigma_m + (\sigma_f - \sigma_m)\frac{v_m}{2}} \right\} = \sigma_m \left\{ \frac{\sigma_m v_m + \sigma_f (1 + v_f)}{\sigma_m (1 + v_f) + \sigma_f v_m} \right\} \tag{5}$$

For an insulating matrix the conductivity is zero ($\sigma_m \approx 0$) and the effective conductivity in a direction perpendicular to the fibers is zero; however, in the direction parallel to the fiber axis, the bulk conductivity is an area weighted average of the fiber conductivity as $\sigma_{par} = \sigma_f v_f$. This term indicates that DC conduction can occur through the composite fibers.

This result implies that the MWM sensor response is directionally dependent and sensitive to the component of the electrical conductivity parallel to the drive windings. Thus, when the sensor is oriented along the length of the fibers the material will behave like a conducting material but in the perpendicular orientation the material will behave like an insulator. Of course, the size of the weave pattern with respect to the sensor geometry is also a factor, but if the sense element is small or comparable to the weave dimensions for the fabric tows and the sensor spatial wavelength is also relatively small, then spatial variations in the composite properties should be observed.

To get a better understanding of the expected behavior for the measured responses, finite element model (FEM) calculations were performed for an FA28 MWM-Array. These simulations assumed 16 fabric plies, with each ply having two fiber orientations to represent the fabric and a ply thickness of 0.009-in. The orientation of each ply was varied to represent the alternating ply orientations in the layup. A fiber volume fraction of 0.60 and lift-offs of 0.0254 mm (0.001-in.) and 0.254 mm (0.010-in.) were assumed.

Figure 14 shows the results of these calculations plotted on a coarse conductivity/lift-off measurement grid. These measurement grids assumed an infinite half-space of isotropic material and provide effective properties for the composite. As the fiber conductivity is reduced the effective conductivity of the composite is also reduced. **The effective conductivity is approximately equal to one-half of the fiber conductivity multiplied by the volume fraction of the fibers.** The sensor response for the 90º orientation (sensor drive perpendicular to surface fibers) tends to have a higher lift-off as the effective conductivity of the composite layer closest to the sensor is zero. This orientation also tends to have the highest effective conductivity. The sensor responses obtained for the 0º orientation (sensor drive parallel to surface fibers) and the 45º orientation are similar since the effective conductivity of the composite layers near the sensor are similar.

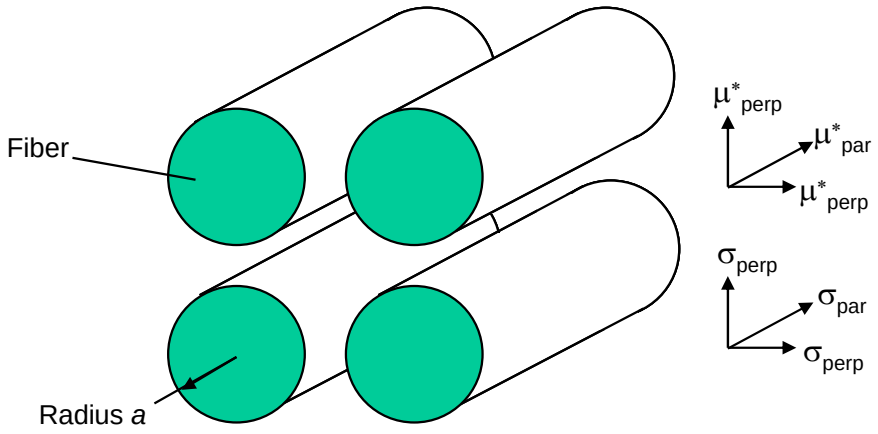

Figure 13. The effective complex permeability and conductivity for a composite structure depends upon the fiber orientation and the properties and dimensions of the fibers and matrix.

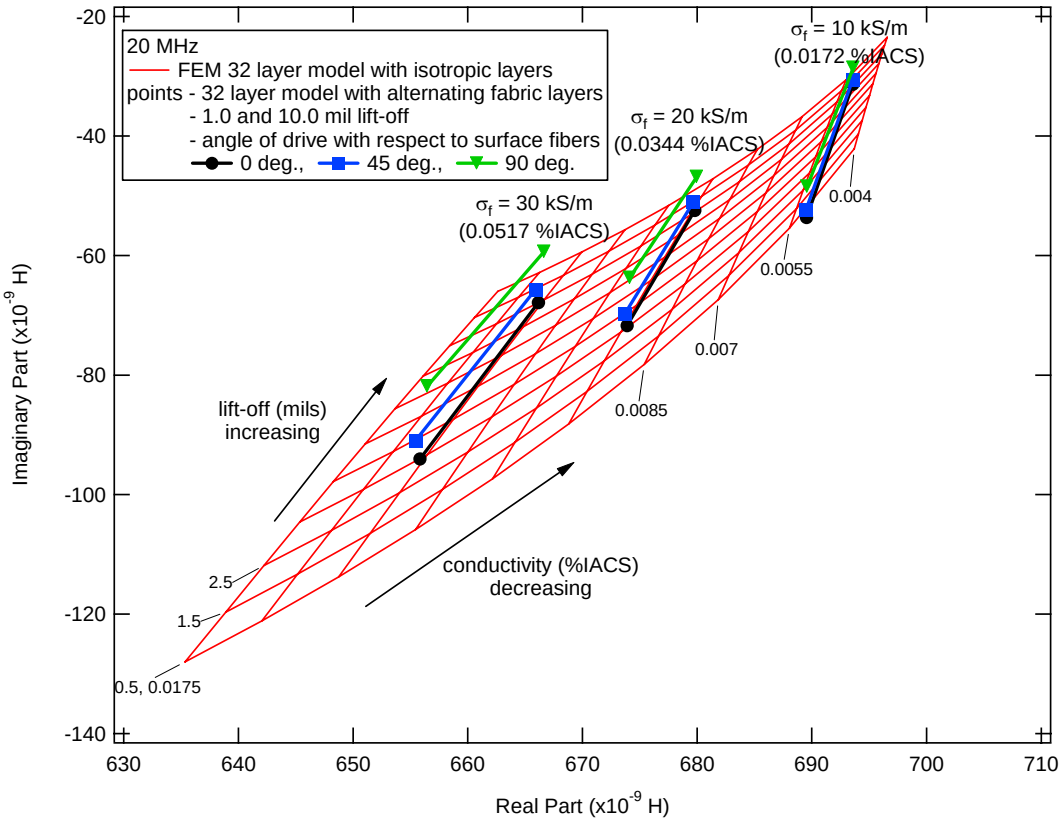

Figure 14. FA28 grid (in red) and anisotropic micromechanical model responses (in green, blue and black).

5. CONCLUSIONS

This paper showed that magnetic field-based eddy current sensors can be used to examine for impact damage or monitor stress in graphite fiber composite materials. In addition, a micromechanical model was presented that can be used to obtain insight into the constituent properties being monitored with the NDE method. For graphite fiber epoxy composites and eddy-current methods, the sensor response depends upon the sensor orientation with respect to the conducting fibers, the electrical conductivity and volume fraction of the fibers, and the thicknesses of the fabric layers. Measurements on several composite panels allowed the fiber

conductivities to be determined and images of the panels showed the fiber tows. High spatial resolution images of the panels are suitable for composite damage evolution modeling and sequential scanning of small and large spatial wavelength sensors over an impact event site allowed subsurface damage to be identified.

This type of model-based NDE approach should improve life management of composite structures. For damage evolution models for composites, the mechanical properties of the matrix and the fibers need to be specified along with the loading source, boundary conditions and initial damage or damage precursor conditions. In some situations the damage can be determined directly by the NDE method, such as the presence of a delamination from an NDE image, but in other situations the NDE information is correlated to the mechanical state. For example, for uniaxial graphite fiber/epoxy composites, the composite conductivity has been found to decrease linearly with low tensile stress but non-linearly for high strain levels where there appears to be (non-reversible) fiber cracking and damage accumulation [7]. Another study showed an increase in composite conductivity with low tensile stress, possibly as a result of stress relaxation in the fibers [5], which suggests that monitoring the absolute electrical conductivity of the fibers can be used to assess the stress in the fibers themselves. Although the paper focused on eddy current methods as it applies to graphite fiber/epoxy composites, the approach is suitable for other NDE methods that can be modeled, such as dielectrometry, ultrasonics and thermography.

6. ACKNOWLEDGEMENTS

This work was partly supported by SBIR funding from the U.S. DoD and NASA. The authors would like to thank Lockheed Martin for providing the composite panels. All conclusions are those of the authors and not the sponsoring agencies.

7. REFERENCES

1. John D. Russsell, “Composite Affordability Initiative: Transitioning Advanced Aerospace Technologies through Cost and Risk Reduction,” The AMMTIAC Quarterly, Vol. 1, No. 3.
2. N. J. Goldfine, “Uncalibrated, Absolute Property Estimation and Measurement Optimization for Conducting and Magnetic Media Using Imposed ω-k Magnetometry,” Doctoral Thesis, Massachusetts Institute of Technology, Cambridge, MA, 1990.
3. N. Goldfine, V. Zilberstein, A. Washabaugh, D. Schlicker, I. Shay, D. Grundy, “Eddy Current Sensor Networks for Aircraft Fatigue Monitoring,” *Materials Evaluation*, Vol.61, No.7, July 2003, pp. 852-859.
4. N. Goldfine, Y. Sheiretov, D. Schlicker, A. Washabaugh, “Rapid, Nonlinear “System” Identification for NDT, Using Sensor Response Databases,” *Materials Evaluation*, Vol. 66, No. 7, July 2008.
5. X. Wang, X. Fu, D.D.L. Chung, “Electromechanical study of carbon fiber composites,” Journal Mater. Res., Vol. 13, No. 11, Nov. 1998, pp. 3081-3092.
6. Z. Hashin, “Analysis of Properties of Fiber Composites with Anisotropic Constituents,” Journal App. Mech. Vol. 46, No. 3, 1979.
7. J.B. Park, T. Okabe, N. Takeda, W.A. Curtin, “Electromechanical modeling of unidirectional CFRP composites under tensile loading condition,” Composites: Part A 33 (2002) 267-275.